Available online at www.sciencedirect.com
ScienceDirect
Journal of Power Sources 171 (2007) 696–705
JOURNAL OF POWER SOURCES
www.elsevier.com/locate/jpowsour

# A mathematical model of a tubular solid oxide fuel cell with specified combustion zone

Junxi Jia [a,*], Abuliti Abudula [b], Liming Wei [c], Renqiu Jiang [a], Shengqiang Shen [d]

[a] College of Power and Energy Engineering, Harbin Engineering University, Harbin 150001, China
[b] New Energy Technology Research Division, Aomori Industrial Research Center, 4-11-6 Daini-tonyacho, Aomori 030-0113, Japan
[c] School of Electric and Electronic Information Engineering, Jilin Architectural and Civil Engineering Institute, Changchun 130021, China
[d] School of Energy and Power Engineering, Dalian University of Technology, Dalian 116024, China

Received 11 June 2007; accepted 15 June 2007
Available online 23 June 2007

**Abstract**

A numerical model has been developed to simulate the effect of combustion zone geometry on the steady state and transient performance of a tubular solid oxide fuel cell (SOFC). The model consists of an electrochemical submodel and a thermal submodel. In the electrochemical model, a network circuit of a tubular SOFC was adopted to model the dynamics of Nernst potential, ohmic polarization, activation polarization, and concentration polarization. The thermal submodel simulated heat transfers by conduction, convention, and radiation between the cell and the air feed tube. The developed model was applied to simulate the performance of a tubular solid oxide fuel cell at various operating parameters, including distributions of circuits, temperature, and gas concentrations inside the fuel cell. The simulations predicted that increasing the length of the combustion zone would lead to an increase of the overall cell tube temperature and a shorter response time for transient performance. Enlarging the combustion zone, however, makes only a negligible contribution to electricity output properties, such as output voltage and power. These numerical results show that the developed model can reasonably simulate the performance properties of a tubular SOFC and is applicable to cell stack design.


*Keywords:* Tubular solid oxide fuel cell; Electrochemical reaction; Heat and mass transfer; Combustion zone

## 1. Introduction

A fuel cell is a device that converts chemical energy into electricity directly through the electrochemical reaction of a fuel (for example, hydrogen) with oxygen. Compared with traditional thermal-electricity generators, a fuel cell is not only more efficient but also more environmentally friendly because of low or zero pollution produced [1,2]. Planar and tubular geometric configurations are the two typical designs for SOFCs. There have been over 40 years of theoretical, laboratory, and modeling studies of tubular SOFCs, a longer time than for planar SOFCs [3]. The technique of design and manufacture of tubular SOFCs is relatively mature [3].

Most experimental investigations have focused on the overall electrochemical performance [4,5], while computational modeling has focused on systematic characteristics at various operation conditions. Because of their validity, calibrated numerical models are expected to be able to achieve system optimization for both steady state and transient performances.

Various models have been developed to simulate tubular SOFC performance [3,4,6–20]. The features of these models are different. Some are steady state models [3,4,6–11]; others are models [12–20] addressed to transient operations.

In general, the electrochemical models of tubular SOFCs include three polarizations: ohmic polarization, activation polarization and concentration polarization. Hirano et al. [4] developed a model to examine the roles of ohmic and concentration polarizations on electrochemical properties with the assumption that the effects from activation polarization were negligibly small. By contrast, the model Aguiar and Chadwick developed [7] did not include concentration polarization because

* Corresponding author. Tel.: +86 451 8254 2449; fax: +86 451 8254 2449.
*E-mail address:* jiajunxi99@sohu.com (J. Jia).

0378-7753/$ – see front matter © 2007 Elsevier B.V. All rights reserved.
doi:10.1016/j.jpowsour.2007.06.057

**Nomenclature**

| | |
|---|---|
| $A$ | area ($m^2$) |
| $C$ | concentration ($mol\ m^{-3}$) |
| $D$ | diffusion coefficient ($m^2\ s^{-1}$) |
| $E_{act}$ | activation energy ($J\ mol^{-1}$) |
| $F$ | Faraday constant ($96485\ C\ mol^{-1}$) |
| $\Delta G$ | change in Gibbs free energy ($J\ mol^{-1}$) |
| $i$ | current density ($A\ cm^{-2}$) |
| $i_0$ | exchange current density ($A\ m^{-2}$) |
| $i$ | current (A) |
| $J_i$ | transport rate of specie $i$ ($mol\ m^{-2}\ s^{-1}$) |
| $K$ | heat exchange coefficient ($W\ m^{-2}\ K^{-1}$) |
| $L$ | length of cell (m) |
| $p$ | partial pressure |
| $r$ | cell radius coordinate (m) |
| $R$ | universal gas constant ($8.314\ J\ mol^{-1}\ K^{-1}$) |
| $V$ | terminal voltage (V) |
| $U_f$ | fuel utilization |
| $U_o$ | oxidant utilization |
| $W$ | electrical power (W) |
| $x$ | cell axial coordinate (cm) |
| $X_i$ | molar fraction of specie $i$ |
| $z$ | electrons transferred per reaction |

*Greek letters*

| | |
|---|---|
| $\alpha$ | transfer coefficient |
| $\varepsilon$ | porosity |
| $\eta$ | polarization (V) |
| $\lambda$ | thermal conductivity ($W\ m^{-1}\ K^{-1}$) |
| $\rho$ | specific resistivity ($\Omega\ cm$) |
| $\tau$ | tortuosity |

*Subscripts*

| | |
|---|---|
| a | anode |
| act | activation polarization |
| air | air in the air feed tube |
| b | air feed tube |
| c | cathode |
| con | concentration polarization |
| cz | combustion zone |
| e | electrolyte |
| g | gas |
| ohm | ohm polarization |
| s | cell solid structure |

the principal electrochemical reactions were considered to be kinetically controlled. Therefore, only activation polarizations were taken into account. For heat transfer, some models have simply considered taking heat conduction and convention into account to simulate the thermal properties: for example, the models developed by Hirano et al. [4] and Campanari and Iora [8]. Radiation, which plays an important role in heat transfer when the temperature of the cell tube is high [3], has been rarely studied.

Achenbach [21,22] developed a transient model for SOFCs that included ohmic, activation and concentration polarizations and radiation heat transfer. M.A. Khaleel et al. [23] numerically analyzed the performance of SOFCs at steady state and at startup using a model that did not take radiation heat transfer into account. Both models were used to simulate the operation of planar SOFCs, not tubular SOFCs. The simulation results from these models showed the overall performance characteristics of the modeled fuel cell to be reasonably estimated. The computational time was also acceptable.

Nonetheless, it is clear that little attention has been paid to the effects of fuel cell geometry on performance or model design. It is also recognized that the effect of the combustion zone geometry on fuel cell performance has seldom been examined either experimentally or numerically. Theoretically, the heat transfer through the combustion zone should play an important role on fuel cell performance because of the large temperature difference produced. For example, when tubular SOFCs work in a cell stack, the unreacted fuel can flow into the combustion zone to react with the depleted air. The combustion products form the exhaust and the heat from the combustion zone can be used to preheat the inlet air.

In this work, a model was developed to simulate the operation of a tubular SOFC with a specified combustion zone. The electrochemical model includes all three polarizations: ohmic, activation and concentration. The radiation between the cell tube and the air feed tube was also included in the thermal model. The effect of the combustion zone geometry on the steady state and transient operation performance of the cell was analyzed in detail.

## 2. Model description

### 2.1. Cell configuration

Fig. 1 illustrates the configuration of the SOFC stack. A tubular SOFC with combustion zone is shown in Fig. 2.

Fuel enters near the outside of the closed end of the cell and flows along the cell to the open end. Air is provided to the inside of the cell via an air feed tube and moves to the closed end of the cell. Oxygen in the air fed to the cathode accepts

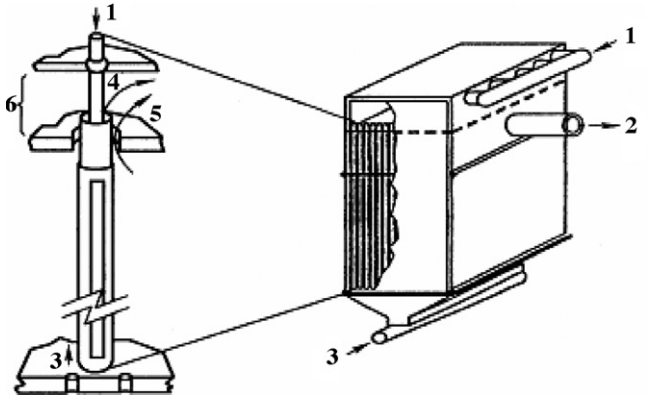


Fig. 1. Scheme of the SOFC stack. (1) Air; (2) exhaust; (3) fuel; (4) unreact air; (5) unreact fuel; (6) combustion zone.

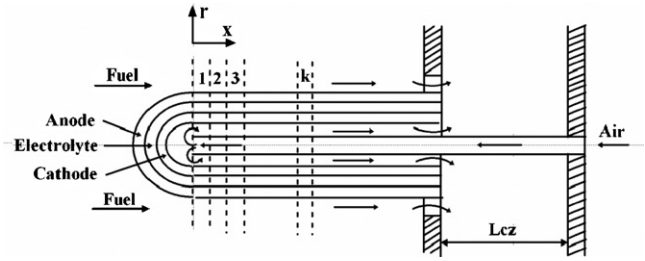


Fig. 2. Configuration of tubular SOFC with combustion zone.

Table 1
Geometry parameters of the tubular SOFC

| Component | Value |
|---|---|
| Thickness of cathode | 2200 μm |
| Thickness of anode | 100 μm |
| Thickness of electrolyte | 40 μm |
| Thickness of air feed tube | 1 mm |
| Outer diameter of cell | 22 mm |
| Outer diameter of air feed tube | 12 mm |
| Length of cell | 150 cm |

electrons from external circuit to form oxygen ions. The ions are conducted through the solid electrolyte to the anode. At the fuel electrode, the ions combine with hydrogen in the fuel to form water. Electrons flow from the anode through the external circuit back to the cathode. Since the electrochemical is exothermic, the cell produces heat as well as electricity.

After exiting the cell, the fuel and air mix and react in the combustion zone. The combustion products flow along the outside of the air feed tube to preheat the incoming air.

The dimensions of the cell and each cell component are listed in Table 1 [24,25].

### 2.2. Electrochemical model

To simulate the electrochemical characteristics of the cell, the tubular cell is divided into slices by the planes perpendicular to $x$-axis as shown in Fig. 2 and denoted by sliced cell. The Nernst potential, electrical current, and polarizations of each slice are calculated individually. A circuit composed of electromotive forces and cell impedances models a sliced cell. Fig. 3 shows the cell equivalent electric circuit.

The cell terminal voltage is constant because the electrode materials are good electric conductors and the resistance of Ni felt used for the electrical contact between cells is sufficiently low. However, the driving Nernst potential varies along the cell length. The varying Nernst potential produces varying local current densities. The nonuniform current results in locally varying voltage polarizations. Each local Nernst potential is reduced to the terminal voltage by the sum of the local voltage polarizations. Therefore, the cell terminal voltage is given by

$$V = E_0 - \eta_{\mathrm{act,a}} - \eta_{\mathrm{act,c}} - \eta_{\mathrm{ohm}} - \eta_{\mathrm{con,a}} - \eta_{\mathrm{con,c}} \quad (1)$$

where $V$ is the cell potential and $E_0$ is the Nernst potential, which is calculated by

$$E_0 = \frac{-\Delta G_0}{2F} + \frac{RT}{2F} \ln \frac{p_{\mathrm{H_2}} (p_{\mathrm{O_2}})^{1/2}}{p_{\mathrm{H_2O}}}. \quad (2)$$

#### 2.2.1. Activation polarization

The development of electrochemical reaction requires overcoming an activation energy barrier. This phenomenon defined as activation polarization can be described by the Bulter-volmer equation [26].

$$i = i_0 \left\{ \exp\left(\frac{\alpha z F \eta_{\mathrm{act}}}{RT}\right) - \exp\left[\frac{-(1-\alpha) z F \eta_{\mathrm{act}}}{RT}\right] \right\} \quad (3)$$

where $\alpha$ is the transfer coefficient, $z$ the number of electrons participating in the electrode reaction, $F$ the Faraday constant, and $i_0$ is the exchange current density that can be calculated as

$$i_{0,\mathrm{a}} = \gamma_{\mathrm{a}} \left(\frac{p_{\mathrm{H_2}}}{p_{0,\mathrm{a}}}\right) \left(\frac{p_{\mathrm{H_2O}}}{p_{0,\mathrm{a}}}\right) \exp\left(-\frac{E_{\mathrm{act,a}}}{RT}\right) \quad (4)$$

$$i_{0,\mathrm{c}} = \gamma_{\mathrm{c}} \left(\frac{p_{\mathrm{O_2}}}{p_{0,\mathrm{c}}}\right)^{0.25} \exp\left(-\frac{E_{\mathrm{act,c}}}{RT}\right) \quad (5)$$

Values for $\gamma_{\mathrm{a}}$, $\gamma_{\mathrm{c}}$, $E_{\mathrm{act,a}}$, $E_{\mathrm{act,c}}$ could be found from literature [26].

#### 2.2.2. Ohmic polarization

Ohmic losses occur because of resistance resulting from the flow of ions in the electrolyte and the flow of electrons through the electrode.

Due to the symmetric current flow through the two halves of the cell in Fig. 4, it is only necessary to calculate the resistance

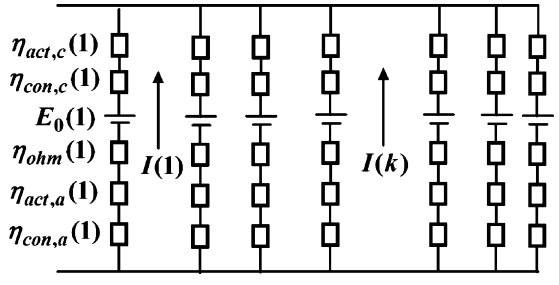


Fig. 3. Cell equivalent electric circuit.

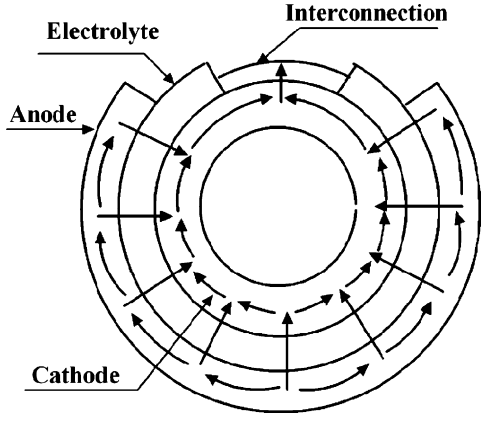


Fig. 4. Current path of tubular SOFC.

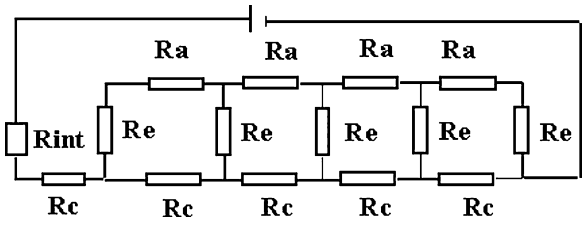


Fig. 5. Equivalent electric circuit of the ohmic resistance.

of a half slice. The total resistance of a cell slice is the parallel combination of the two halves. The equivalent electric circuit of the ohmic resistance for calculation is given in Fig. 5.

The cell equivalent ohmic resistance depends on the anode, cathode and electrolyte resistances.

Ohmic polarization is expressed by Ohm's law:

$$\eta_{\text{ohm}} = I\sum R_i \tag{6}$$

where $R_i = \rho_i\delta_i/A_i$ is the ohmic resistance of anode, cathode, and electrolyte in each share of the equivalent circuit of Fig. 5, $A_i$ the respective area of the section where the current flows, $\delta_i$ the corresponding current flow length and $\rho_i$ is the material resistivity, which is the strong function of temperature as given in Table 2 [1,3].

### 2.2.3. Concentration polarization

The analysis of concentration polarization should begin with the analysis of the transport of gases through porous electrodes. The electrode concentration overpotential considers the difference in gas concentrations between the electrode–electrolyte interface and the bulk. Mass transport models inside the porous SOFC electrode must be applied to estimate gas concentrations at the electrode–electrolyte interface. In this model, both ordinary and Knudsen diffusions are considered. The model has taken into account the physical properties of SOFC material like porosity, tortuosity and pore size of the electrode materials. The concentration polarization is given by two terms, related to the anode and cathode side:

$$\eta_{\text{con}} = \frac{RT}{2F}\ln\frac{X^0_{\text{H}_2}X^{\text{r}}_{\text{H}_2\text{O}}}{X^{\text{r}}_{\text{H}_2}X^0_{\text{H}_2\text{O}}} + \frac{RT}{4F}\ln\frac{X^0_{\text{O}_2}}{X^{\text{r}}_{\text{O}_2}} = \eta_{\text{con,a}} + \eta_{\text{con,c}} \tag{7}$$

where $X^0_i$ and $X^{\text{r}}_i$ is the molar fraction of specie $i$ in the bulk and at the electrode–electrolyte interface, respectively, which can be estimated by the Fick's law:

$$J_i = -D_{i,}\frac{\text{d}C_i}{\text{d}r} \tag{8}$$

where $D_i = [\tau/\varepsilon(1/D_{i,\text{m}} + 1/D_{i,\text{k}})]^{-1}$, $D_{i,\text{m}}$ the mass diffusion coefficient of specie $i$ in the mixture, $D_{i,\text{k}}$ the Knudsen diffusion coefficient of species $i$, $\varepsilon$ the porosity and $\tau$ is tortuosity.

Applying the Kirchhoff's law of current, the currents in each share of the equivalent circuit can be obtained [27,28].

## 2.3. Thermal model

### 2.3.1. Energy balance equations in tubular SOFC

The cell temperatures influence the electrochemical model and these temperatures affect the local driving voltage, polarizations, and heat generation within the cell. A thermal model has been developed to determine these temperatures by a finite-volume approach. In the electrochemical model, the cell is divided into axial sections or slices. In the thermal model, the same sections are used and each section is composed of the solid structure, air feed tube and flow passages volumes. Energy balances equations for such volumes in each section can be described as follows.

The general form of the energy conservation equation for a control volume is,

$$\frac{\text{d}E_{\text{CV}}}{\text{d}t} = \dot{Q}_{\text{CV}} - \dot{W}_{\text{CV}} + \sum_i n_i h_i|_{\text{in}} - \sum_i n_i h_i|_{\text{out}} \tag{9}$$

where $E_{\text{CV}}$ is the internal energy ($J$), $\dot{Q}_{\text{CV}}$ the rate of thermal energy ($W$) transferred across the control volume, $\dot{W}_{\text{CV}}$ the rate of work transferred across the control volume, $\sum_i n_i h_i|_{\text{in}}$ the enthalpy gained due to mass flowing into the element, and $\sum_i n_i h_i|_{\text{out}}$ is the enthalpy loss due to mass flowing out of the element. For the steady state, left hand term in Eq. (9) is eliminated.

The change rate of internal energy is given by:

$$\frac{\text{d}E_{\text{cv}}}{\text{d}t} = \rho\cdot C_{\text{V}}\cdot(\Delta V)\cdot\frac{\text{d}T}{\text{d}t} \tag{10}$$

where $\rho$ is the density (kg m$^{-3}$), $C_{\text{V}}$ the specific heat at constant volume (J kg$^{-1}$ K$^{-1}$), $\Delta V$ the elemental volume (m$^3$), $T$ the absolute temperature (K), and $t$ is time (s).

Tracking of the energy flows in the cell proceeds by making separate energy balances for the air in the air feed tube, cathode gas, fuel gas and solid structure.

The energy balances for air preheating volume is expressed as:

$$\rho_{\text{air}}c^{\text{air}}_{\text{V}}\,\Delta V_{\text{air}}\frac{T^{k,p+1}_{\text{air}} - T^{k,p}_{\text{air}}}{\Delta t} = \sum_i n^{k+1,p}_i h^{k+1,p}_i - \sum_i n^{k,p}_i h^{k,p}_i + K_{\text{air}}A_{\text{a}}(T^{k,p}_{\text{b}} - T^{k,p}_{\text{air}}) \tag{11}$$

Table 2
Properties of SOFC components

| | Resistivity (Ω cm) | Pore radius of electrode (μm) | $\tau/\varepsilon$ | Thermal conduction (W m$^{-1}$ K$^{-1}$) | Emissivity |
|---|---|---|---|---|---|
| Cathode | 0.008114 exp(600/$T$) | 1 | 3/30% | 9.6 | 0.9 |
| Electrolyte | 0.00294 exp(10350/$T$) | – | – | 2.7 | – |
| Anode | 0.00298 exp(−1392/$T$) | 1 | 3/30% | 6.23 | — |
| Air feed tube | – | – | – | 6.04 | 0.9 |

where $K_{air}$ is the convective heat transfer coefficient between the air preheating and air feed tube and $A_a$ is the heat transfer area, $p$ is the time index and $\Delta t$ is the change in time from time step $p$ to time $p+1$.

For the full developed laminar flow, the heat transfer coefficient is expressed by [29]

$$K = Nu\frac{\lambda_g}{D_e}$$

where $\lambda_g$ is the thermal conductivity of the mixed gas, $D_e$ the equivalent diameter.

The cathode gas energy balance can be written as

$$\rho_c c_V^c \Delta V_c \frac{T_c^{k,p+1} - T_c^{k,p}}{\Delta t} = \sum_i n_i^{k-1,p} h_i^{k-1,p} - \sum_i n_i^{k,p} h_i^{k,p} + K_{bc} A_c^b (T_b^{k,p} - T_c^{k,p}) + K_{sc} A_c^s (T_s^{k,p} - T_c^{k,p}) - \frac{I_k}{4F} h_{O_2}^{k,p} \quad (12)$$

where $K_{bc}$ is the convective heat transfer coefficient between the cathode gas and air feed tube and $K_{sc}$ is the convective heat transfer coefficient between solid cell and bulk cathode air flow. The last term on the right hand side is the rate of energy accompanying mass transfer of oxygen out of the bulk to the cathode solid.

The time varying energy conservation equation for fuel gas can be written as,

$$\rho_f c_V^f \Delta V_f \frac{T_f^{k,p+1} - T_f^{k,p}}{\Delta t} = \sum_i n_i^{k-1,p} h_i^{k-1,p} - \sum_i n_i^{k,p} h_i^{k,p} + K_{sf} A_f^s (T_s^{k,p} - T_f^{k,p}) - \frac{I_k}{2F} (h_{H_2}^{k,p} - h_{H_2O,T_s}^{k,p}) \quad (13)$$

where the first and the second term on the right hand side are the rates of energy transfer accompanying the fuel mass flow into and out of the element, the third term is the convective heat flux from the solid cell to the fuel gas, and the last term is the sum of the energy accompanying mass transfer of reactant ($H_2$) and reaction product ($H_2O$).

The solid cell unsteady energy balance is written as,

$$\rho_s c_V^s \Delta V_s \frac{T_s^{k,p+1} - T_s^{k,p}}{\Delta t} = \frac{\lambda_s}{\delta x} A_{\lambda s} (T_s^{k-1,p} - T_s^{k,p}) - \frac{\lambda_s}{\delta x} A_{\lambda s} (T_s^{k,p} - T_s^{k+1,p}) + K_{sf} A_f^s (T_f^{k,p} - T_s^{k,p}) + K_{sc} A_c^s (T_c^{k,p} - T_s^{k,p}) - \frac{A_b \sigma [(T_s^{k,p})^4 - (T_b^{k,p})^4]}{1/\varepsilon_b + (A_b/A_s)(1/\varepsilon_s - 1)} - \frac{I_k}{2F} \Delta H_{H_2O,T_s} - W^{k,p} \quad (14)$$

where the former five terms on the right of Eq. (14) are the net energy transferred to the cell by heat transfer via conduction, convection, and radiation. The sixth term is the net energy addition by the convective flux of reacting species to the solid cell and subsequent release of their respective reaction enthalpies. The last term is the electrical energy generated in the solid cell due to electrochemical oxidation of hydrogen.

In the cell region, the equation for the air feed tube is expressed as:

$$\rho_b c_V^b \Delta V_b \frac{T_b^{k,p+1} - T_b^{k,p}}{\Delta t} = \frac{\lambda_b}{\delta x} A_{\lambda b} (T_b^{k-1,p} - T_b^{k,p}) - \frac{\lambda_b}{\delta x} A_{\lambda b} (T_b^{k,p} - T_b^{k+1,p}) + K_{air} A_a (T_{air}^{k,p} - T_b^{k,p}) + K_{bc} A_c^b (T_c^{k,p} - T_b^{k,p}) + \frac{A_b \sigma [(T_s^{k,p})^4 - (T_b^{k,p})^4]}{1/\varepsilon_b + (A_b/A_s)(1/\varepsilon_s - 1)} \quad (15)$$

In the combustion zone, the equations is

$$\rho_b c_V^b \Delta V_b \frac{T_b^{k,p+1} - T_b^{k,p}}{\Delta t} = \frac{\lambda_b}{\delta x} A_{\lambda b} (T_b^{k-1,p} - T_b^{k,p}) - \frac{\lambda_b}{\delta x} A_{\lambda b} (T_b^{k,p} - T_b^{k+1,p}) + K_{air} A_a (T_{air}^{k,p} - T_b^{k,p}) + K_{cz} A_{cz} (T_{cz}^{k,p} - T_b^{k,p}) \quad (16)$$

where the last term on the right of Eq. (16) is the net energy transferred to the air feed tube by heat transfer via convection between the combustion products and the air feed tube.

In the combustion zone, fuel and air that exit the cell mix, combust and are converted to the combustion products flow. The mixture temperature is determined from the energy balance of the exiting gas. The combustion react occurs instantaneously and the combustion heat is generated in a very thin region. Therefore, the heat source is added to the first combustion products node.

The time varying energy conservation equation of the first node for combustion products can be written as:

$$\rho_{cz} c_V^{cz} \Delta V_{cz} \frac{T_{cz}^{k,p+1} - T_{cz}^{k,p}}{\Delta t} = \sum_i n_i^{mix,p} h_i^{mix,p} - \sum_i n_i^{k,p} h_i^{k,p} + K_{cz} A_{cz} (T_b^{k,p} - T_{cz}^{k,p}) - n_{H_2}^{exit} \Delta H_{T,mix}^{com} \quad (17)$$

where the first and the second term on the right hand side of Eq. (17) is the rats of energy transfer accompanying the exit fuel and air mass flow into and out of the element, the third term is the convective heat flux from the air feed tube to the products gas, and the last term is the combustion heat.

The unsteady energy balance of the rest node for combustion product is written as,

$$\rho_{cz} c_V^{cz} \Delta V_{cz} \frac{T_{cz}^{k,p+1} - T_{cz}^{k,p}}{\Delta t} = \sum_i n_i^{k-1,p} h_i^{k-1,p} - \sum_i n_i^{k,p} h_i^{k,p} + K_{cz} A_{cz} (T_b^{k,p} - T_{cz}^{k,p}). \quad (18)$$

### 2.4. Boundary conditions

The boundary conditions for the energy conservation equations are as follows.

As the air feed tube is divided into $n$ sections and the cell tube is divided into $m$ sections, accordingly the combustion zone is divided into $n - m$ sections.

At the entrance of the air and fuel,

$$T_{air}^{n+1} = T_{air}|_{inlet} \quad (19)$$

$$T_f^0 = T_f|_{inlet} \quad (20)$$

The air preheating becomes the cathode gas at the exit of the air feed tube, therefore the continuity between the feed air and the cathode gas can be expressed as,

$$T_{air}^0 = T_c^0 \quad (21)$$

The outlet end of cell and the inlet of the air feed tube are considered adiabatic, that is,

$$T_s^m = T_s^{m+1} \quad (22)$$

$$T_b^n = T_b^{n+1}. \quad (23)$$

### 2.5. Numerical solution algorithm

In a SOFC, current and temperature distributions are strongly coupled. The electrochemical model is solved with a tentative temperature profile. The electrochemical model determines the Nernst potential, current and electric power. The thermal model accepts these results from electrochemical model and calculates the temperature of the gasses and solids. There temperatures are applied to the electrochemical model for the next calculation of cell Nernst potential, current and power. As the simulation progressed the model steps back and forth between electrochemical and thermal calculations until the convergence is obtained. The equations are solved numerically using the Gauss Seidel method.

## 3. Results and discussion

### 3.1. Steady state characteristics

In order to investigate the accuracy of the model, the calculate $V$–$i$ curve is compared with the experimental data in reference [5] in Fig. 6.

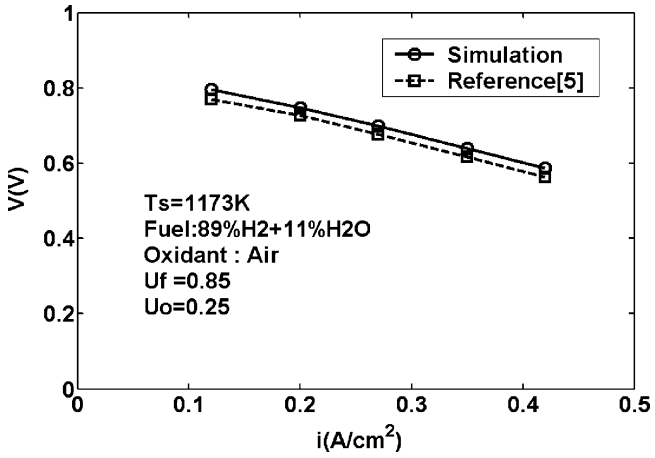


Fig. 6. Cell voltage vs. current density.

Table 3
Condition and parameters for simulation

| | |
|---|---|
| Fuel inlet composition (molar fraction) | 89% $H_2$ + 11% $H_2O$ |
| Oxidant inlet composition (molar fraction) | 21% $O_2$ + 79% $N_2$ |
| Fuel inlet temperature (K) | 1173 |
| Oxidant inlet temperature (K) | 1173 |
| Fuel inlet flow rate (mol $s^{-1}$) | $1.96 \times 10^{-3}$ |
| Oxidant inlet flow rate (mol $s^{-1}$) | $3.73 \times 10^{-2}$ |
| Operation pressure (atm) | 1 |

The relative deviation between the simulated voltage and experimental voltage in reference [5] is no larger than 5%. Such a good agreement for the terminal voltages between the model-prediction and the experiment shows that the present model is reliable.

The operation conditions and parameters for simulation in the work are listed in Table 3.

Fig. 7 shows the temperature profile for the fuel flow ($T_f$), the air in the air feed tube ($T_{air}$), the cathode gas flow ($T_c$), and the combustion product ($T_{cz}$). The temperatures of air in the feed tube and annulus channel increase gradually in the direction of flow due to the heat transferred by convection. The temperature distribution of fuel is dependent on the temperature of cell tube.

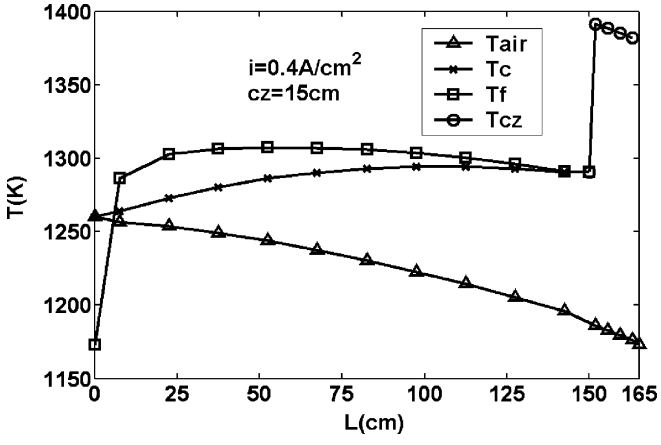


Fig. 7. Temperature profiles of gas in the tubular SOFC.

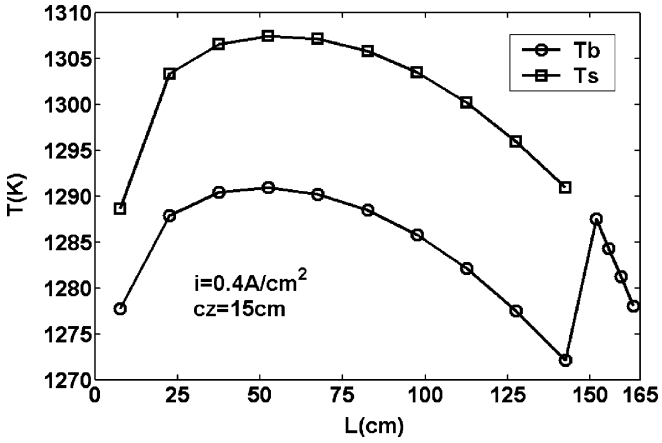


Fig. 8. Temperature profiles of solid in cell.

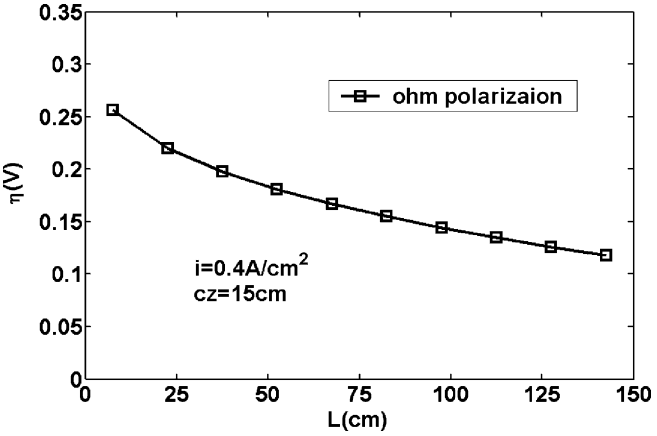


Fig. 10. Ohmic polarization profiles.

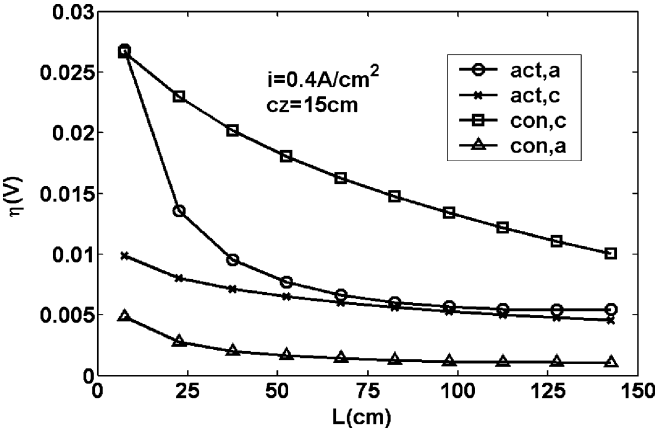


Fig. 11. Activation and concentration polarization profiles with combustion zone.

Due to the exothermic combustion reaction, the temperature of the combustion product has a evident increase from the temperature of mixed gases, then the temperature of it decreases gradually because of the convection on the outside of air feed tube between the hot products and the feed tube.

It is important for the SOFC to work under the maximum temperature limit, however, it is difficult to measure the temperature. In the work, the simulated results for the solid temperature profiles along the *x*-axis are shown in Fig. 8. Both of the temperature of air feed tube and cell solid structure increase and then decreases along the *x*-axis, the two ends of the cell tube have a lower temperature than the middle of the cell tube. The reduced temperatures at the ends are due to heat transfer to the incoming fuel and air. In the combustion zone, the temperature distribution of the air feed tube is affected by feed air cooling and combustion product heating.

Fig. 9 shows the local Nernst voltage and current density. Both of them decrease along the *x*-axis. It is because that along the stream, the depletion of fuel and oxide has a significant effect on the local Nernst voltage.

The three kinds of polarization losses, which decrease the cell potential from the ideal Nernst value to the real value, are shown in Figs. 10 and 11. Among the three polarizations, the ohmic polarization plays the most significant role in the cathode-supported SOFC. The concentration polarization at the anode side is smaller than that at the cathode because the cathode is thicker than anode and the reactant diffuse through the relatively thick porous cathode to the reaction site at the cathode electrolyte interface. The concentration polarization at the anode side is negligible with respect to the other losses.

Fig. 12 shows the molar fractions variation of gases in the cell along the fuel path. The consumption of the fuel gas and

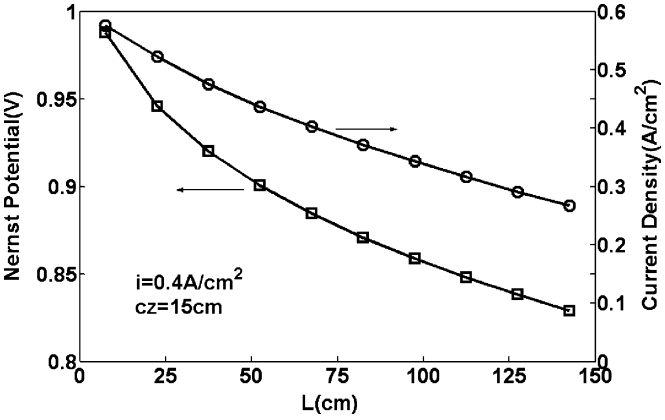


Fig. 9. Nernst voltage and current density profiles.

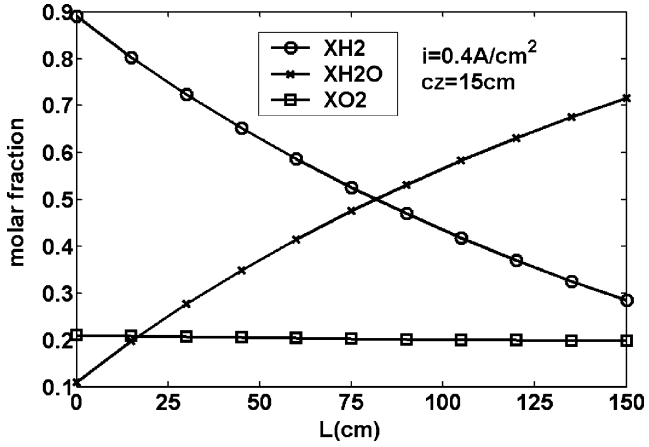


Fig. 12. Flow chemical composition profile.

Table 4
Effect of the length of combustion on the performance of tubular SOFC

| $L_{cz}$ (cm) | 0 | 15 | 0 | 15 | 0 | 15 |
|---|---|---|---|---|---|---|
| $i$ (A cm$^{-2}$) | 0.3 | 0.3 | 0.4 | 0.4 | 0.5 | 0.5 |
| $T_s$, max (K) | 1260 | 1272.4 | 1295.7 | 1307.4 | 1341.1 | 1352 |
| $T_s$, min (K) | 1246.4 | 1258.2 | 1277.7 | 1288.6 | 1313.7 | 1323.5 |
| $\Delta T = T_s$, max-$T_s$, min (K) | 13.6 | 14.24 | 18.0 | 18.75 | 27.4 | 28.53 |
| $T_s$, aver (K) | 1256 | 1268.3 | 1289.5 | 1300.9 | 1331.2 | 1341.6 |
| $V$ (V) | 0.7571 | 0.7602 | 0.6965 | 0.7000 | 0.6404 | 0.6435 |
| $W$ (W) | 130.3 | 130.93 | 159.9 | 160.68 | 183.3 | 184.62 |

oxidant by electrochemical reaction determines the decrease of hydrogen and oxygen along the $x$-axis. Hydrogen and oxygen consumption lead to the formation of water vapor. Therefore, the molar fraction of water shows an increase along the $x$-axis. The excess air is needed to provide air-cooling in SOFC as the allowable temperature rise of the solid cell is limited by the thermal stress induced in the ceramic cell components. Therefore, the change of $O_2$ molar fraction is not so large as that of $H_2$ and $H_2O$.

The effect of the length of combustion on the performance of the tubular SOFC in given in Table 4. For the fixed average current density, all the other input data are assumed as in Table 3. It can be concluded that increasing the length of combustion zone leads to a increasing of cell tube temperature. Although the terminal voltage and cell power also increase due to the increasing of the length of combustion zone, the degree of variation can be ignored.

The effects of the length of the combustion zone on the temperature of the cell tube and inlet air inside the air feed tube at the open end of the cell region are shown in Figs. 13 and 14.

Fig. 14 shows that the longer the combustion zone, the more heat is used to heat the inlet air, which lead to the higher the temperature of the cell tube in Fig. 13. For the same inlet air at the 1173 K, its temperature increase by 0, 18 and 30 K to the 1173, 1191 and 1203 K inside the air feed tube at the open end of the cell on the condition that the length of combustion is 0, 15, 30 cm, respectively.

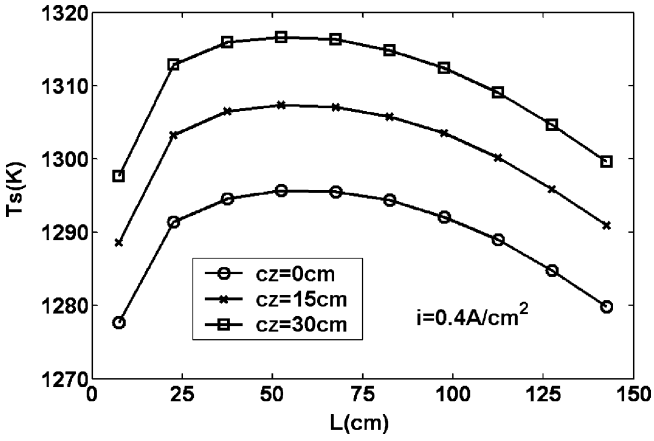


Fig. 13. Effect of the length of combustion zone on the temperature profile of cell tube.

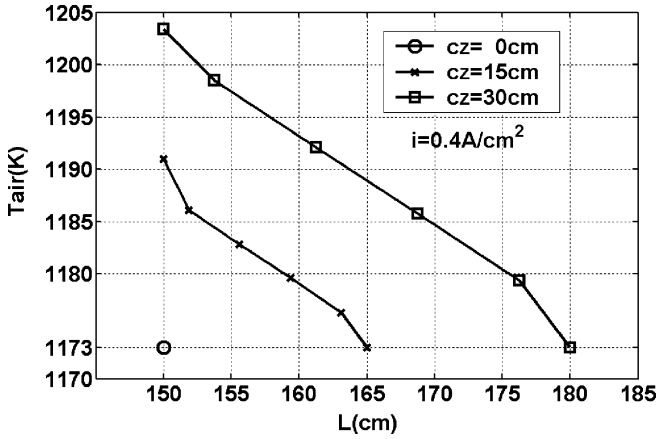


Fig. 14. Effect of the length of combustion zone on the temperature of inlet air inside the air feed tube at open end of the cell.

### 3.2. Transient simulation

In order to investigate the transient behavior of the tubular SOFC with combustion zone, the transient electrical response and the temperature profile of the solid structure have been simulated as the average current density increase from 0.4 to 0.5 A cm$^{-2}$ at $t = 0$ s as shown in Fig. 15. During the simulation, the inlet temperature and flow rates of fuel and oxidant are kept constant, all the other parameters are assumed as in Table 3.

Figs. 16 and 17 show the transient terminal voltage and power profile for the cell. The maximum, minimum and average temperatures of the solid structure are shown in Fig. 18 during

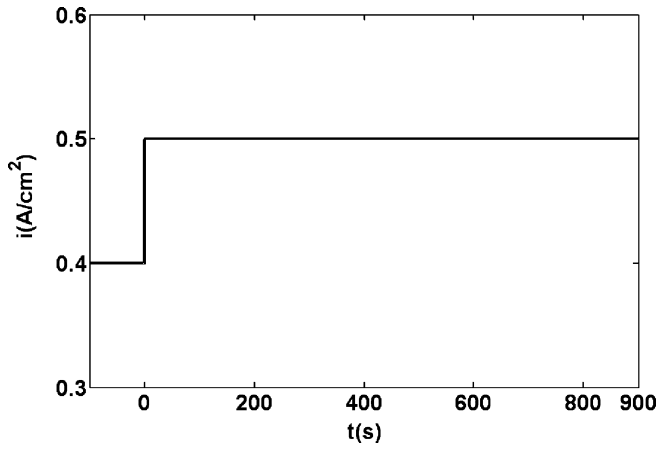


Fig. 15. Step increase in cell current density.

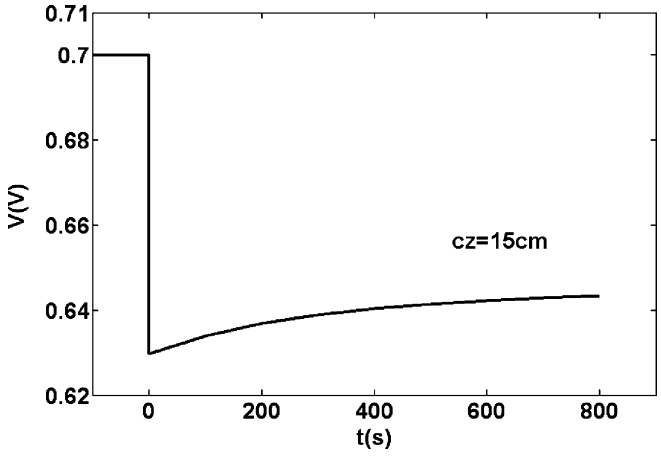


Fig. 16. Terminal voltage response due to current step increase.

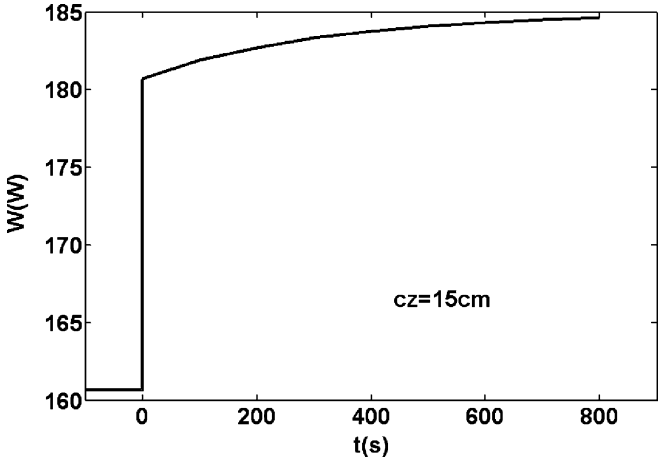


Fig. 17. Output power response due to current step increase.

the transient for $i = 0.4\,\mathrm{A\,cm^{-2}}$ up to $i = 0.5\,\mathrm{A\,cm^{-2}}$. The step increase of the average current results in the increase of the power output of cell. The temperatures of cell solid structure also increase due to the load change. These temperatures show a decaying type of growth toward their finial values. The time

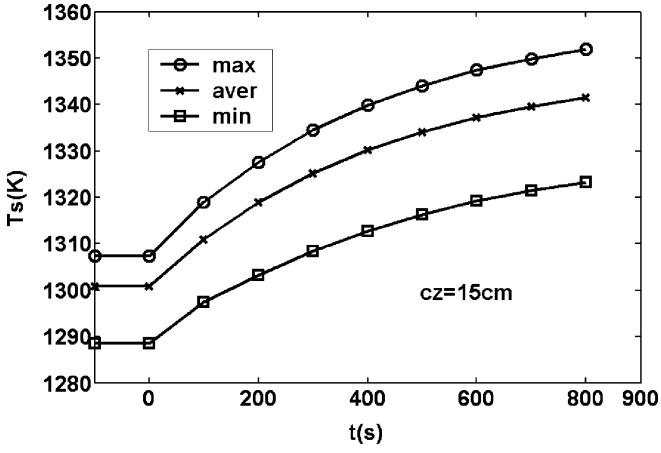


Fig. 18. Max, min and average temperature response of the solid structure due to current step increase.

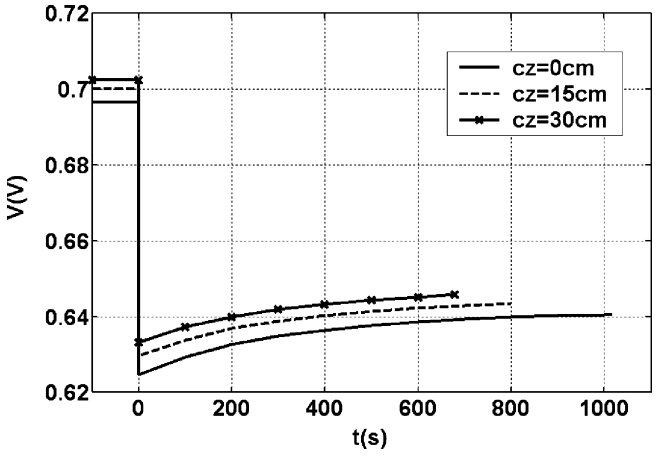


Fig. 19. Terminal voltage response due to current step increase.

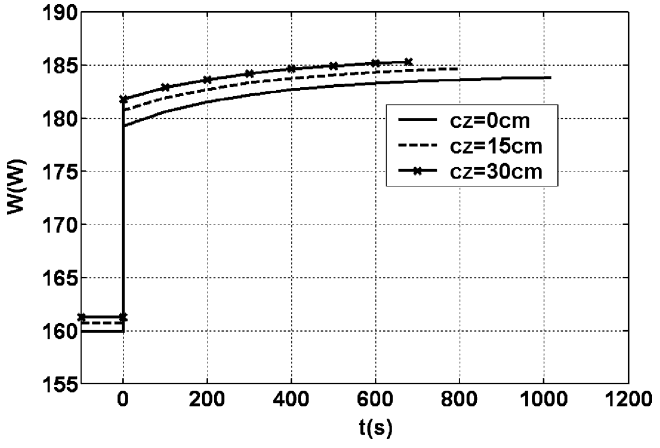


Fig. 20. Output power response due to current step increase.

from the old steady state to the new one is about 800 s. These curves show the same trends as those presented in [21,22] for the planar stack.

For the same step increase in current density from 0.4 to $0.5\,\mathrm{A\,cm^{-2}}$, the effect of the combustion zone length on the transient electrical response is shown in Figs. 19 and 20. For the combustion zone which length is 0, 15 and 30 cm, the time to reach the new steady state is, respectively 1017, 800 and 679 s.

## 4. Conclusions

A model has been developed to simulate the steady state and transient characteristics of a tubular SOFC with specified combustion zones. The electrochemical model was designed to evaluate the ohmic, activation and concentration polarizations. The thermal model includes heat transfer by conduction, convention, and radiation. The current distributions, gas concentration distribution and temperature distribution were also simulated by the model. The influence of the combustion zone length was analyzed in terms of both the steady state and transient characteristics.

The results showed that ohmic polarization represents the highest loss among the three polarizations in a cathode-

supported tubular SOFC, at least one order of magnitude greater than the other losses. The middle part of the SOFC has a relatively higher temperature than that at either end of the fuel cell.

It is found that by increasing the combustion zone length, the overall temperature of the cell tube increased, while the terminal voltage and the output power hardly changed. In terms of the transient response, increasing the length of combustion zone led to a quicker response of the cell from one steady state to another. None of the previously published tubular SOFC models have addressed the effects of combustion zone geometry on the steady state and transient performance of the cell.

## References


[1] A.F. Massardo, F. Lubelli, J. Eng. Gas Turbine Power 122 (2000) 27–35.
[2] P. Costamagna, L. Magistri, A.F. Massardo, J. Power Sources 96 (2001) 352–368.
[3] N.F. Bessette II., W.J. Wepfer, J. Winnick, J. Electrochem. Soc. 142 (1995) 3792–3800.
[4] A. Hirano, M. Suzuki, M. Lppommatsu, J. Electrochem. Soc. 139 (1992) 2744–2751.
[5] S.C. Singhal, Solid State Ionics 135 (2000) 305–313.
[6] S. Nagata, A. Momma, T. Kato, J. Power Sources 101 (2001) 60–71.
[7] P. Aguiar, D. Chadwick, Chem. Eng. Sci. 57 (2002) 1665–1677.
[8] S. Campanari, P. Iora, J. Power Sources 132 (2004) 113–126.
[9] P.-W. Li, M.K. Chyu, J. Power Sources 124 (2003) 487–498.
[10] P.-W. Li, L. Schaefer, M.K. Chyu, J. Heat Transfer 126 (2004) 219–229.
[11] T.W. Songa, J.L. Sohna, J.H. Kimb, T.S. Kimc, S.T. Roa, K. Suzukid, J. Power Sources 142 (2005) 30–42.
[12] R. Suwanwarangkul, E. Croiset, M.D. Pritzker, M.W. Fowler, P.L. Douglas, E. Entchev, J. Power Sources 154 (2006) 74–85.
[13] D.J. Hall, R.G. Colclaser, IEEE Trans. Energy Conv. 14 (1999) 749–753.
[14] T. Ota, J. Power Sources 118 (2003) 430–439.
[15] J. Jia, S. Shen, Chem. Res. Chin. Univ. 21 (2005) 577–582.
[16] P. Aguiar, C.S. Adjiman, N.P. Brandon, J. Power Sources 147 (2005) 136–147.
[17] P. Nehter, J. Power Sources 157 (2006) 325–334.
[18] J. Padulles, G.W. Ault, J.R. McDonald, J. Power Sources 86 (2000) 495–500.
[19] K. Sedghisigarchi, A. Feliachi, IEEE Trans. Energy Conv. 19 (2004) 423–428.
[20] X. Xue, J. Tang, N. Sammes, Y. Du, J. Power Sources 142 (2005) 211–222.
[21] E. Achenbach, J. Power Sources 49 (1994) 333–348.
[22] E. Achenbach, J. Power Sources 57 (1995) 105–109.
[23] M.A. Khaleel, Z. Lin, P. Singh, W. Surdoval, D. Collin, J. Power Sources 130 (2004) 136–137.
[24] R.A. George, N.F. Bessette, J. Power Sources 71 (1998) 131–137.
[25] J.H. Hirsochenhofer, D.B. Stauffer, R.R. Engelmen, M.G.S. Klett, Fuel Cell Handbook, fifth ed., U.S. Department of Energy, Office of Fossil Energy, Morgantown, West Virginia, 2000.
[26] P. Costamagna, K. Honnegger, J. Electrochem. Soc. 145 (1998) 3995–4007.
[27] J. Jia, S. Shen, et al., Acta Energiae Solaris Sinica 25 (2004) 457–461.
[28] J. Jia, S. Shen, S.B. Riffat, M. Gillott, J. Energy Institute 78 (2005) 76–80.
[29] W.M. Keys, M.E. Crawford, Convective Heat and Mass Transfer, second ed., McGraw-Hill, New York, 1980.